Asymmetric Vortices on a Slender Body of Revolution

G. G. Zilliac,* D. Degani,† and M. Tobak‡
NASA Ames Research Center, Moffett Field, California 94035

The symmetric and asymmetric leeward-side flowfields on an inclined ogive cylinder have been investigated using a number of experimental techniques. Naturally occurring and perturbed flowfields were studied at a moderate Reynolds number and at many incidence angles. By close examination of the steady side-force behavior at different roll orientations of the tip, it has been established that microvariations in the tip geometry of the model have a large influence on the downstream development of the flowfield. Under certain conditions a bistable flowfield was observed.

Nomenclature

C_p = pressure coefficient
C_y = side force coefficient, $Y/(0.5\rho U_\infty{}^2 S)$
D = maximum diameter of body
f = frequency, Hz
L = length of body
Rn_D = Reynolds number based on D
S = model base area, $\pi(D/2)^2$
U_∞ = freestream velocity
X = distance from nose in axial direction
Y = side force
α = angle of attack
ρ = density
ϕ = circumferential roll angle measured from windward ray

Introduction

RECENTLY, some insights have been gained into the nature of the steady and unsteady flows generated by pointed bodies of revolution at incidence. These insights have come as a result of a synergy of experiments and computations. In Ref. 1 the unsteady aspects of the flowfield generated by an inclined $L/D = 16$ ogive-cylinder model were studied. Particular attention was paid to the high-frequency shear-layer fluctuations that were previously computed[2] and also to the effect of incidence angle on the periodic shedding of vortices. During the wind-tunnel experiments, many questions arose concerning the factors that influence vortex shedding and the existence of an asymmetric stationary mean flow. These questions, in turn, have been the motivation both for the present experimental investigation and for the computational studies reported in Refs. 3 and 4.

In Refs. 3 and 4 a three-dimensional time-accurate Navier Stokes code was used to investigate the time-dependent flowfields of ogive cylinders ($L/D = 6.5$ to $L/D = 12.5$) at several angles of attack. At $\alpha = 40$ deg, the mean flow was found to be symmetric. Placement of a small space-fixed and asymmetrically disposed perturbation near the tip of the model caused the mean flow to become asymmetric. Upon removal of the perturbation, the mean flow returned to a symmetric state. At $\alpha = 80$ deg, a short-time-duration perturbation was used as a trigger. Vortex shedding was initiated by the perturbation and continued at approximately the same level well after perturbation was removed.

The objectives of this paper are to investigate the sensitivity of the leeside flowfield to geometrical alterations in light of the results of Refs. 1–4 and additionally to provide some relevant information concerning several issues that have been raised by the results of previous investigators. The pertinent issues consist of the following.

First, does the flowfield have a bistable state, and, if so, under what conditions? Results of an experiment performed by Lamont[5,6] indicated that a purely bistable condition did not exist. The ogive-cylinder model ($L/D = 15$) used by Lamont was heavily instrumented, and the forebody (first $7.5D$) could be rolled by remote control. The side force was determined by the integration of time-averaged surface pressure measurements. At $\alpha = 55$ deg, the side-force variation with roll angle (square wave in appearance) seemed to indicate bistable behavior, yet there were some points that fell between the two side-force extremes at the values of roll angle where a switchover occurred. We will attempt to clarify the nature of these seeming anomalous points.

Second, does a "regular" (most frequently occurring) vortex configuration occur? Dexter and Hunt[7,8] studied a flowfield similar to the one studied here, and also similar to that of Ref. 5, and found that there were regular values of the local side-force coefficient that were sustained over large changes in roll angle. In addition, when the vortex pattern was in its regular configuration, the local side-force-coefficient magnitude measured at each position along the body was greater than that measured at all other roll angles. Two regular configurations were found, corresponding to a right-hand and left-hand vortex pattern. Under certain conditions crossover or intermediate regions were observed where the vortices were not in either configuration. The experiment involved rolling the model and measuring the circumferential pressure distribution at 10 X/D positions along the body ($Rn_D/\sin\alpha = 1.0 \times 10^5$) for angles of attack between 35 and 65 deg. The pressure distributions were integrated to determine the local side-force-coefficient variation with roll angle, X/D position, and α. A controversial conclusion of this study, which we will examine, was that two wind-tunnel model noses, produced to the same machining tolerances, will produce the same regular-state side-force magnitude (with different roll-angle trends).

Third, is the geometry of the model nose the greatest factor in determining the leeward-side vortex orientation? Dexter and Hunt[7,8] found that the roll orientation of the nose dominated the flow development and that the roll-angle orientation of the cylindrical afterbody had little effect on the flow.

Presented as Paper 90-0388 at the AIAA 28th Aerospace Sciences Meeting, Reno, NV, Jan. 8–11, 1990; received Jan. 26, 1990; revision received June 20, 1990; accepted July 5, 1990.

*Research Scientist. M.S. 260-1, NASA Ames Research Center, Moffett Field, CA 94035.

†Associate Professor, on leave from Technion IIT, Dept. of Mechanical Engineering, Haifa, Israel. Associate Fellow AIAA.

‡Staff Scientist. M.S. 227-4, NASA Ames Research Center, Moffett Field, CA 94035. Associate Fellow AIAA.

This finding is contradicted by the results of Keener,[9] who investigated the aerodynamic characteristics of various combinations of noses, forebodies, and afterbodies at different roll angles and angles of attack up to 58 deg. Keener's results showed that the side-force coefficient varied significantly with the roll angle of the cylindrical afterbody while a constant nose roll-angle position was maintained on a three-piece (nose, forebody, afterbody) $L/D = 10.5$ ogive-cylinder model. Similar results were obtained for a two-piece model. We will attempt to resolve this seeming contradiction.

Fourth, does the size, location, and type of space-fixed perturbation affect the level of asymmetry? In an attempt to understand the importance of the nose geometry, the effects of nose bluntness, roughness, and surface perturbations were studied in Ref. 10. The main conclusion of this investigation was that machining imperfections could be the principal drivers of flowfield asymmetries. The authors also concluded that there was a maximum level of asymmetry that could occur at a given angle of attack and that this level was not affected by nose bluntness. We will examine these conclusions in light of the experiences gained here.

Fifth, what happens to the leeward-side vortices emanating from the nose at large incidence angles? At higher angles of attack (> 65 deg for $L/D = 15$ and longer), the flow becomes unsteady. Ramberg[11] studied the flowfield on pointed bodies of L/D up to 100 and angles of attack to 90 deg and illuminated the unsteady flowfield behavior in a series of beautiful flow-visualization photos. Two distinctive shedding frequencies were measured: one associated with the nose region, and a lower shedding frequency associated with the cylindrical part of the body (also see Ref. 1). Also associated with the nose, a stationary asymmetric component of the flow was observed, and it is of interest to determine its nature.

The attempt to resolve these issues will result, we hope, in a body of experimental information that, when used in conjunction with Ref. 1, will form a detailed and self-consistent data set for comparison with computational and theoretical results.

Experimental Approach

Aerodynamic force measurements and wake velocity measurements were performed in a 38 × 38 cm low-turbulence wind tunnel (Fig. 1) at a velocity of 21 m/s. Based on this velocity and the maximum diameter of the axisymmetric wind-tunnel model, the Reynolds number Rn_D was equal to 30,000. The model configuration studied consisted of an $L/D = 3.5$ ogive with an $L/D = 12.5$ cylindrical afterbody. Overall length of the model was 34.9 cm, and the diameter (D) of the cylindrical afterbody portion of the model was 2.16 cm. As depicted in Fig. 2, the ogive tip could be rotated by a microstepping motor. The model and stepping motor were mounted on a Task Corp. 1.91-cm MRK XII six-component strain-gauge balance.

As pointed out by several researchers,[5-8] model vibration can influence the measurement of the mean flow properties. To minimize this possibility, a viscous damper consisting of a piece of honeycomb immersed in a pot of glycerin was installed to reduce the amplitude of model vibrations (shown in Fig. 2). The damper reduced model vibration amplitudes to an equivalent level that is less than the freestream turbulence level (maximum of $\Delta u/U_\infty = 0.15\%$) of the wind tunnel. Worst-case tip vibration was less than ±0.16 mm at a natural frequency of 10 Hz ($\Delta\beta' = \pm 0.009$ deg). Balance calibration curves obtained with and without the damper present showed no measurable side-force differences, indicating that the applied damping was pure.

Inherent in the operation of strain-gauge balances is a wind-tunnel model deflection that is proportional to the force being measured. Under the conditions of the present test, the true mean sideslip angle, during a roll sweep, varied by a maximum of 0.018 deg. This level of sideslip-angle variation is significantly less than the cross-stream flow-angle variation of the empty wind tunnel (up to 0.5 deg). At several points during the experiment, the model was intentionally set at a small positive or a small negative sideslip angle (0.25 deg) to check the influence of sideslip. The differences between measurements with and without intentionally set sideslip were minimal.

During the preliminary design stages of this experiment, significant balance force interactions were anticipated owing to the relatively small side forces being measured in comparison to the normal-force tare loads. An in situ calibration apparatus (shown in Fig. 2) was designed and constructed to cope with this possibility. In practice, the degree of balance-force interactions was found to be small. In addition, the balance side-force calibration remained essentially constant during the experiment. Periodically, the 20-point calibration curves were checked using the calibration rig. The differences were found to be within the uncertainty of the side-force measurements.

An uncertainty analysis of the side-force measurements was conducted that included the effects of calibration errors and analog-to-digital (A/D) sampling errors. The principal error source was found to be the uncertainty in the applied calibration loads. Results of the analysis were that the side force could be in error by up to 0.09 N. It is believed that the error analysis is conservative because of an overestimation of the calibration load uncertainty and that the actual error is closer to 0.02 N. This figure was determined from checking the re-

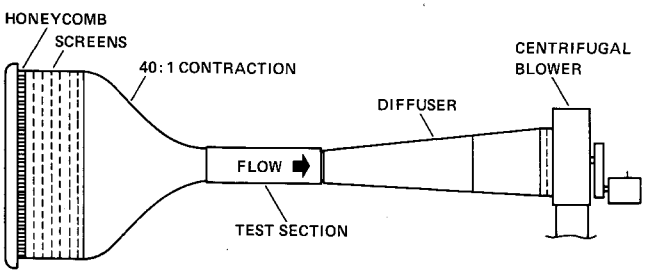

Fig. 1 Plan view of the 38 × 38 cm wind tunnel.

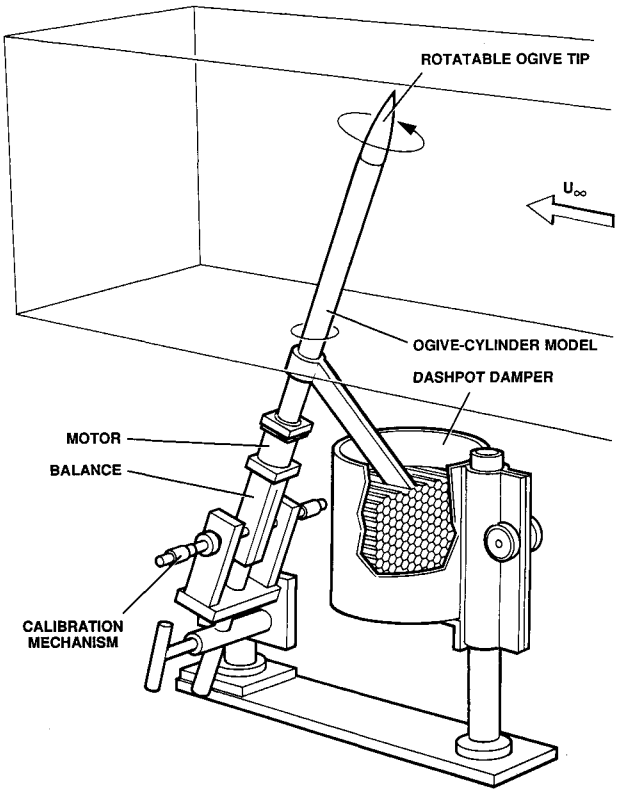

Fig. 2 Perspective view of the ogive-cylinder model.

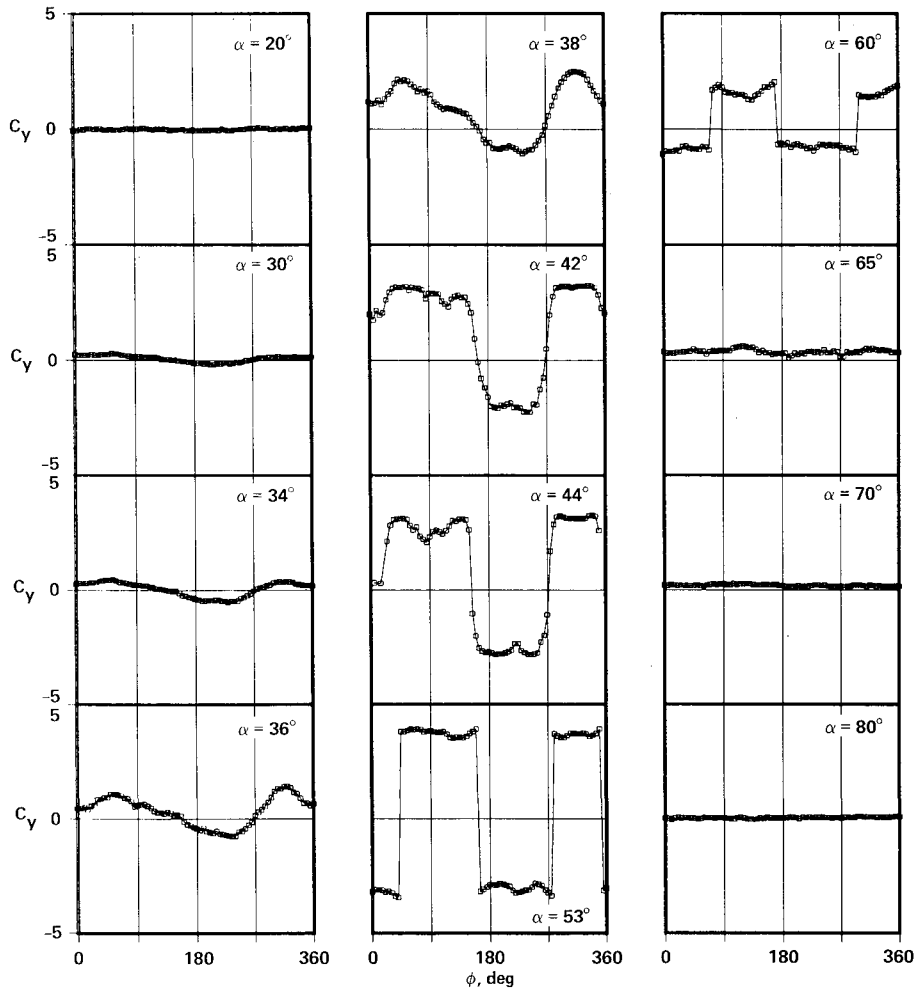

Fig. 3 Side force vs nose roll angle (natural tip): Rn_D = 30,000.

peatability of many measurements under different conditions and on different days and by comparison with the results of other researchers. Under the conditions of the present test 0.02 N corresponds to a side-force coefficient error of $\Delta C_y = 0.25$.

At a high angle of attack (> 60 deg), where the mean side force should be zero, a small side force was measured. It is believed that the source of this anomalous side force was a slight misalignment of the balance, which caused a component of either the normal or chord force to be reflected in the side-force measurements. This small offset (up to $C_y = 0.4$) was subtracted from the side-force data presented in the following sections.

Primary instrumentation used in the study included two channels of Newport Corp. model 2000 transducer conditioner (bridge and amplification), a Krohn-Hite model 3342R filter unit, a Hewlett-Packard 3582A spectrum analyzer, a microVax II computer with 12-bit A/D, and a Disa model 55M10 hot-wire anemometer.

Signals from the two wind-tunnel balance side-force gauges were low-pass filtered at 1 Hz. A minimum of 2000 samples over a sampling period of 2 s were taken and processed. The raw A/D counts were checked for steadiness during the sampling period. If the A/D counts varied by more than 10%, the sampling period was automatically increased (up to a maximum of 8 s). If no steady value was found, the extremes of the side-force variation were recorded and the data point was discarded.

As will be discussed in the following section, it was found that a small accumulation of dust on the tip of the model could greatly alter the force characteristics. The practice became to wipe the tip of the model lightly with dry lens tissue prior to each new angle-of-attack condition.

The flowfield was visualized by means of smoke and a laser light sheet (2.5-W laser). Smoke (kerosene vapor) was introduced at the front of the wind-tunnel contraction via a rake that produced 33 filaments. The plane-of-symmetry images were photographed using a 35-mm camera with a shutter speed of up to 1/2000 s and ASA 3200 film that was pushed two stops. The vertical-cross-plane images were taken using a shutter speed of 1/60 s and ASA 135 film.

Some of the results presented are cases with spatial perturbations on the tip of the model. The technique for applying one of the perturbations involved stringing a 0.008-cm wire between two supports and attaching the wire to the tip of the model. Under a microscope the wire was brought into contact with the tip, and a small drop of solder was applied. Nitric acid etching was then used to cut the wire to the desired length. This approach made it possible to apply a perturbation of known size and orientation.

No boundary-layer trips were used to stabilize the vortex positions or cause boundary-layer transition. Maximum wind-tunnel model blockage, based on the projected frontal area of the model, was less than 5.0% of the cross-sectional area of the test section at a 90-deg angle of attack.

Results

Measurements were made at a Reynolds number of 30,000 and at angles of attack ranging from 20 to 90 deg. Pressure transducer measurements and smoke visualization showed that the flow separation was laminar and the line of separation was located circumferentially approximately 90 deg from the windward ray.

Figure 3 shows the side-force variation with nose roll angle at several incidence angles for the model with unaltered (natural) tip. As can be seen, the side force is virtually zero at all roll angles at $\alpha = 20$ deg and nearly so at $\alpha = 30$ deg, im-

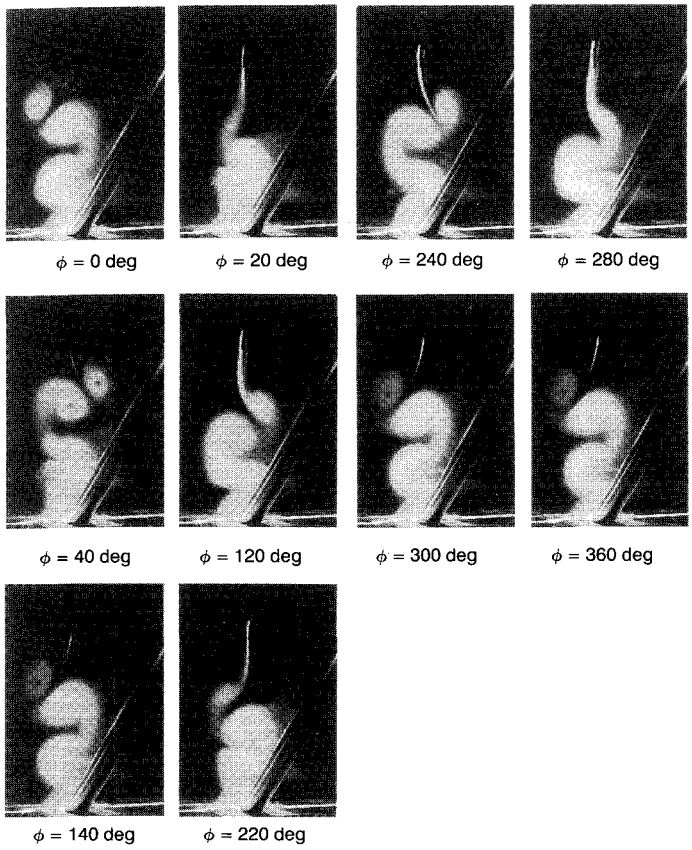

a) Visualized leeward-side flowfield

b) Side force vs nose roll angle

Fig. 4 Smoke laser sheet visualization of flowfield: α = 40 deg; Rn_D = 30,000.

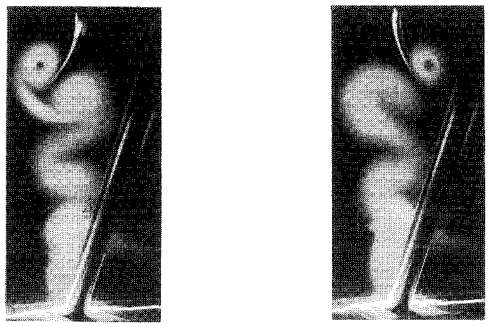

a) Left-hand configuration: C_y = 3.79

b) Right-hand configuration: C_y = −3.57

Fig. 5 Smoke laser sheet visualization of flowfield: α = 55 deg; Rn_D = 30,000.

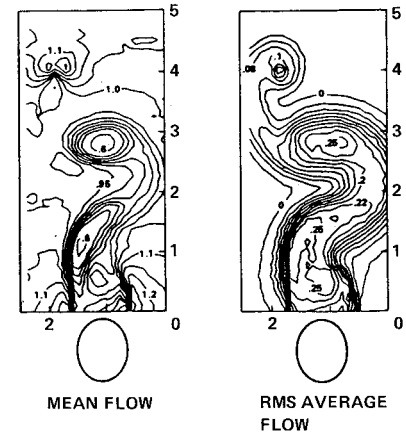

Fig. 6 Hot-wire survey of a plane: X/L = 0.55; α = 55 deg; Rn_D = 26,000 (from Ref. 1).

plying that the leeward-side vortex orientation is virtually symmetric at these low values of α. As the angle of attack is increased from 34 to 42 deg, the magnitude of side-force variation with nose roll angle grows.

Figure 4 shows a correlation of the side-force measurements with visualizations of the corresponding flowfield, the latter made possible by means of smoke and a laser sheet in a vertical plane at X/L = 1.0 and α = 40 deg. As might be expected, there is a succession of leeward-side vortex orientations, each corresponding to a different value of side force. Although unimportant to the point of Fig. 4, the side-force trend presented in Fig. 4b does not agree well with the trend presented in Fig. 3. The reason for this discrepancy is that, during a previous run, the tip of the model was contaminated by a smoke stream. Prior to the present run, a thorough job of cleaning the nose was not done.

With an increase of incidence angle from 42 to 53 deg, the rate of growth of the side-force extremes tapers off and the character of the variation with nose roll angle changes from a continuous distribution to one approaching a square-wave distribution. As the trend toward a square-wave distribution develops, the number of data points found in the vicinity of the zero-crossings diminishes. At α = 53 deg, a nearly pure bistable condition is evident and the side-force extremes are at their maxima. Unlike the visualization at α = 40 deg, at α = 55 deg, the leeward-side flowfield has only two orientations (left-hand and righthand), as shown in Fig. 5. A frame-by-frame videotape analysis of the visualized flowfield indicated that it took approximately 0.1 s for the flowfield to re-establish itself after a switch in orientation.

The hot-wire survey results in Fig. 6 show that the flowfield has two distinct streamwise vortices that emanate from the tip. In the area between the tip vortices and the body, a region of

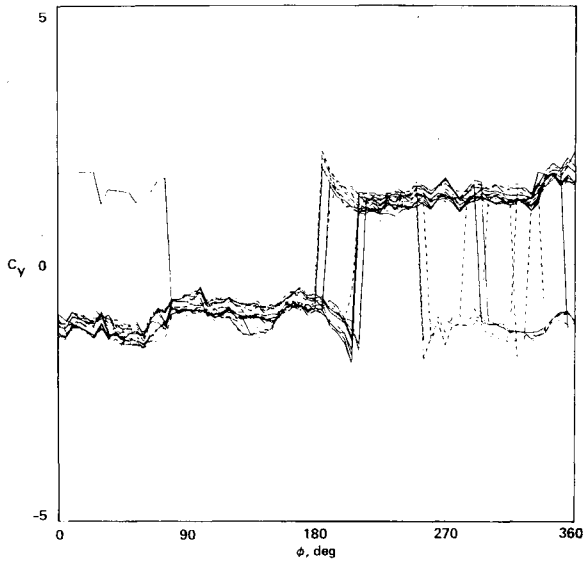

Fig. 7 Multiple roll sweeps; α = 60 deg.

velocity deficit and also high rms fluctuations exists where additional streamwise vortices of low strength may be present.

At α = 60 deg, an interesting behavior was observed. Repeat runs involving rotations in both the $+\phi$ and $-\phi$ directions produced different zero crossings with every nose-roll-angle sweep. At first it was thought that this was evidence of hysteresis, but on closer examination the possibility was rejected because the apparent hysteresis loop was not repeatable. Multiple runs with ϕ sweeps in both directions were carried out at each incidence angle, and the side-force data repeatability was found to be within the experimental error for all incidence angles studied with the exception of 60 deg (see Fig. 7).

The mean side-force variation with nose roll angle at incidence angles of 65 deg and greater is virtually zero. As reported in Ref. 1, α = 65 deg was the incidence angle where the first evidence of periodic vortex shedding was detected.

Figure 8 gives smoke/laser sheet visualizations of the flow in the leeward-side symmetry plane of the model. The images were taken using a fast shutter speed (1/2000 s) in order to freeze the unsteady wake. It is difficult to make out the precise details of the flowfield, but several features are evident. At α = 70 deg, alternating bands of dark (no smoke) and light (smoke), which are inclined with respect to the axis of the model, are present. These are the periodically shed vortices. Near the top of the frame, two nearly streamwise smoke streaks, emanating from the tip of the model, are evidence of the pair of tip vortices seen previously in the hot-wire survey results (Fig. 6). With increasing incidence angle (α = 80 and 90 deg), the shed vortices become more closely aligned with the body axis and the tip vortices become less evident.

Other evidence of the highly sensitive nature of the flowfield was observed. Early in the study, it was found that, at all angles of attack, the trends of side force vs nose roll angle would change over a period of time. A close look at the nose under a microscope revealed that dust particles (approximately 3 μm diam) had coated the nose. Cleaning the nose with lens tissue eliminated the problem. An example of the degree to which dust could influence the magnitude of the side force is shown in Fig. 9. This figure shows a comparison of the side force for the model with an accumulation of dust (circles) and the model after a tip cleaning (squares).

It was also observed that smoke particles (approximately 1 μm diam) generated by the vaporization of kerosene could have a similar effect on the flowfield if the smoke stream were allowed to hit the tip. In fact, with a continuous stream of smoke particles hitting the tip, it was impossible to measure a steady side force at α = 40 deg. When the smoke rake was positioned so that no filaments hit the nose, little to no effect on the side-force distribution was found.

A test was performed to check the effect of sideslip on the flowfield. The model was set at sideslip angles of 0.25, 0.0, and -0.25 deg at an incidence angle of 40 deg. The results show a minor effect on the side-force variation (see Fig. 10).

The sensitivity of the flowfield to small perturbations located in the vicinity of the tip is a well-known phenomenon. In addition, it is known that the size and location of disturbances at the tip also greatly affect the level of asymmetry (see Ref. 10). What is still not understood is why the flowfield becomes asymmetric, and why it is so sensitive to the tip geometry. To address these questions from another aspect, a series of tests were performed that involved geometrical alterations of the tip. This approach was taken with the hope of being able to affect the flow in a predictable manner and hence assist in the development of a theoretical model of the flowfield.

The first geometrical alteration involved placing a very small cylinder on the nose of the model, perpendicular to the axis of the body and aligned with the ϕ = 0 deg direction. Figure 11 shows the side-force variations with nose roll angle at a succession of angles of attack. Several differences between results for the natural nose (cf. Fig. 3) and those for the deliberately altered nose are immediately apparent. As the angle of attack is increased from 20 deg, extremes of the side-force magnitude increase at a greater rate for the altered nose than for the natural nose. At α = 53 deg, the side-force extremes for the altered nose reach their maxima and are approximately the same magnitude as those for the natural nose. With a further increase in angle of attack, an unexpected side-force behavior occurs. Intermediate values of side force are observed in contrast to the earlier findings of a bistable state under these conditions. It appears that the addition of the wire has fundamentally altered the flowfield. At α = 65 deg, steady side-force measurements were unobtainable during the first half of the nose rotation cycle, indicating that the leeward-side flowfield did not have a stable mean.

The goal of achieving a predictable form of the side-force variation with nose roll angle was not fully realized. Given the new tip geometry, it was hoped that side-force zero-crossings would be forced to occur with every 90-deg change in tip roll angle (crossings at ϕ = 0, 90, 180, and 270 deg) corresponding to the symmetry planes of the model with respect to the angle-of-attack plane. It turned out that only three of the four zero crossings occurred as anticipated, with the fourth occurring at ϕ = 120 deg instead of ϕ = 90 deg. Although great care was taken in attaching the wire to the tip of the model, a small bump on the wire, at approximately half the distance between the model tip and one end of the wire, was observed under a microscope. This bump would have caused a small geometrical asymmetry on the windward side of the model at ϕ = 90 deg that may have been the source of the shift of the zero crossing to ϕ = 120 deg. At ϕ = 270 deg, the bump would have been on the leeward side and may have been unable to influence the flowfield, thereby failing to disrupt the symmetry required for a zero crossing.

A last ditch effort was made to achieve full side-force regularity by machining two precise, symmetrically disposed, microscopic flats at 45 deg with respect to the model axis on the tip of the model. As shown in Fig. 12, the side-force trends with nose roll angle and angle of attack are very regular for this tip configuration. The anticipated zero crossings at ϕ = 0, 90, 180, and 270 deg were achieved. The side-force results also indicate a nearly bistable behavior similar to the natural nose at α = 53 and 60 deg. One interesting aspect of these results is the tendency of the side-force magnitude to diminish abruptly to a lower level in the intervals between zero crossings (note spikelike behavior on either side of a zero crossing). This behavior is evident at all angles of attack and is particularly evident at α = 55 deg.

Interpretation of Results

Leeside Flowfield Development

The features that we think are essential are clearly evident in the set of flow-visualization photographs presented by Ramberg[11] and also to a degree in Figs. 4, 5, and 8. We urge the reader to consult these pictures together with our interpretation of them in the ensuing discussion.

It simplifies matters to consider first the flow past an inclined pointed cylinder that is infinitely long. There are three distinct regimes of flow (cf. Fig. 13). The first is far enough downstream from the nose that its influence on the flow there is negligibly small. Accordingly, the flow in regime 1 is essentially the flow past an inclined cylinder, for which the independence principle[12] holds. In the crossflow direction normal to the cylinder axis, we have simply the two-dimensional flow past a cylinder. Regimes 2 and 3 overlap and are influenced by the nose. In regime 2 the periodic time-dependent shedding of vortices continues as before, but here the vortices are inclined obliquely to the cylinder axis. Regime 3 is the steady asymmetric component.

In Ramberg's experiments, which involved bodies of high fineness ratio ($L/D \sim 100$), all three regimes are easily identifiable in the flow-visualization pictures, although the extent of regime 1 diminishes rapidly as α approaches zero. In experimental studies involving bodies of lower fineness ratio, such as the one studied here ($L/D = 16$), the flow is dominated by regimes 2 and 3 at low to moderate values of α, with regime 1 being virtually nonexistent. Its presence becomes identifiable only after α has become sufficiently large (here, $\alpha \sim 65$ deg) and becomes predominant as α approaches 90 deg, squeezing regimes 2 and 3 into an ever-diminishing zone just behind the nose (see Fig. 8).

Angle-of-Attack Regimes

Experimental results confirm the existence of four angle-of-attack regimes that categorize the types of vortex behavior to be expected on pointed bodies of revolution of finite length. At low angles of attack ($\alpha < 30$ deg), the flowfield is steady and symmetric relative to the angle-of-attack plane. In an intermediate angle-of-attack range (30 deg $< \alpha <$ 50 deg), the flowfield is essentially composed of regime 3: steady and asymmetric. At higher values of α, the steady asymmetric component becomes nearly bistable. For values of α greater than about 65 deg, the flowfield consists of regimes 2 and 3 over the forward part of the body and regime 1 over the aft part of the body. The existence of regimes 1 and 2 is characterized by the presence of two distinctive frequencies: one associated with the oblique shedding of vortices on the

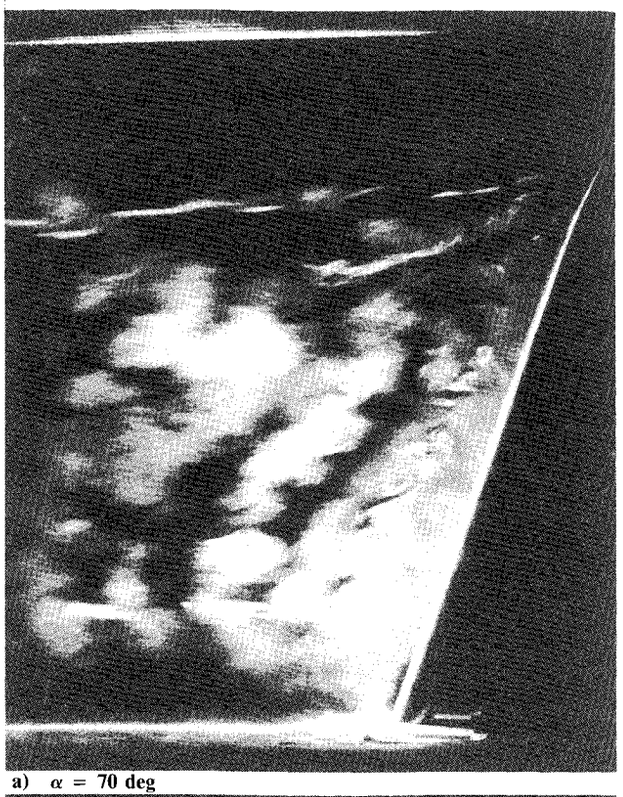

a) α = 70 deg

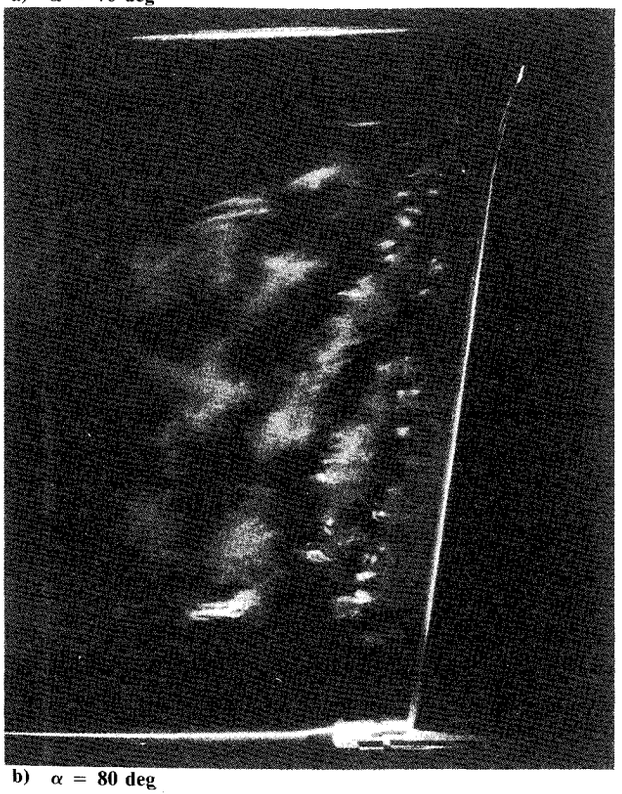

b) α = 80 deg

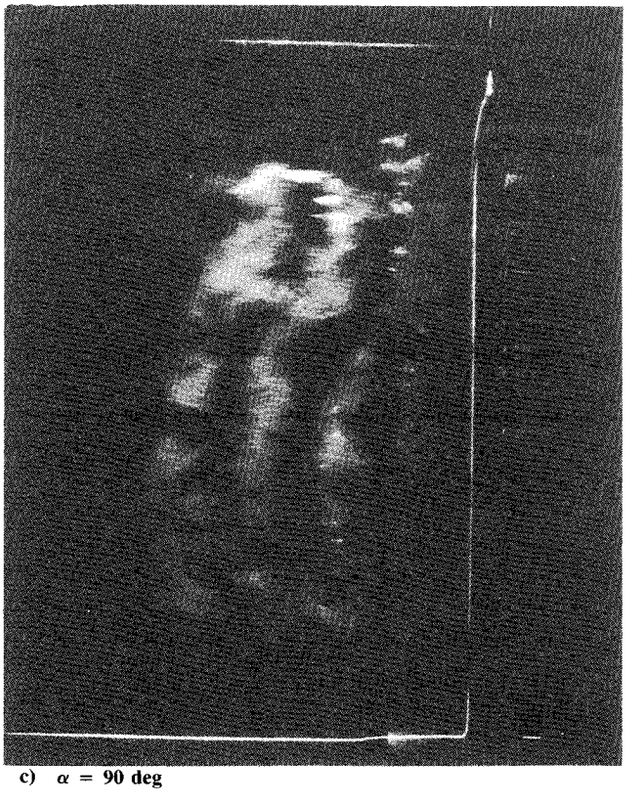

c) α = 90 deg

Fig. 8 Smoke laser sheet visualization of flowfield: Rn_D = 30,000.

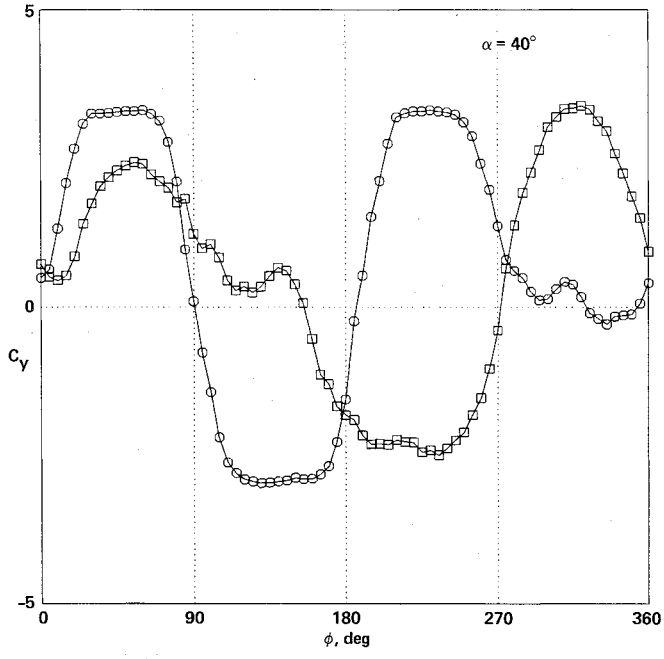

Fig. 9 Effect of dust particles on the side-force variation; α = 40 deg.

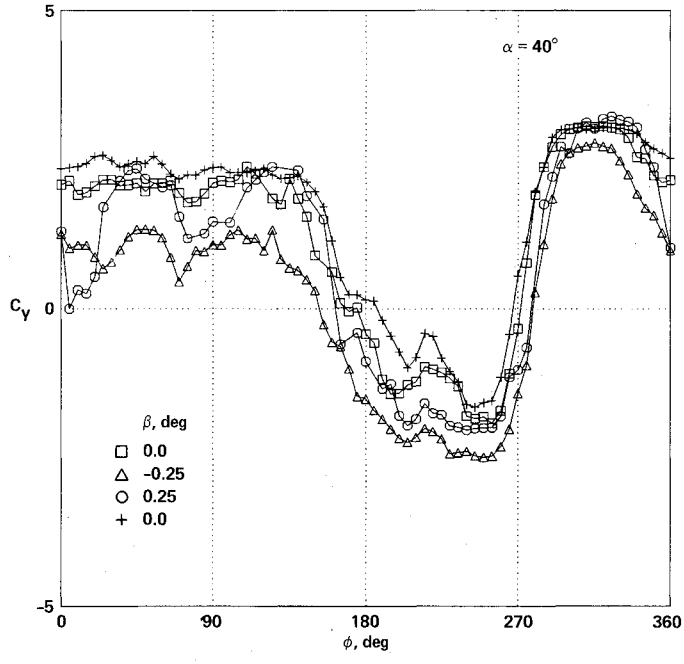

Fig. 10 Effect of sideslip angle on the side-force variation; α = 40 deg.

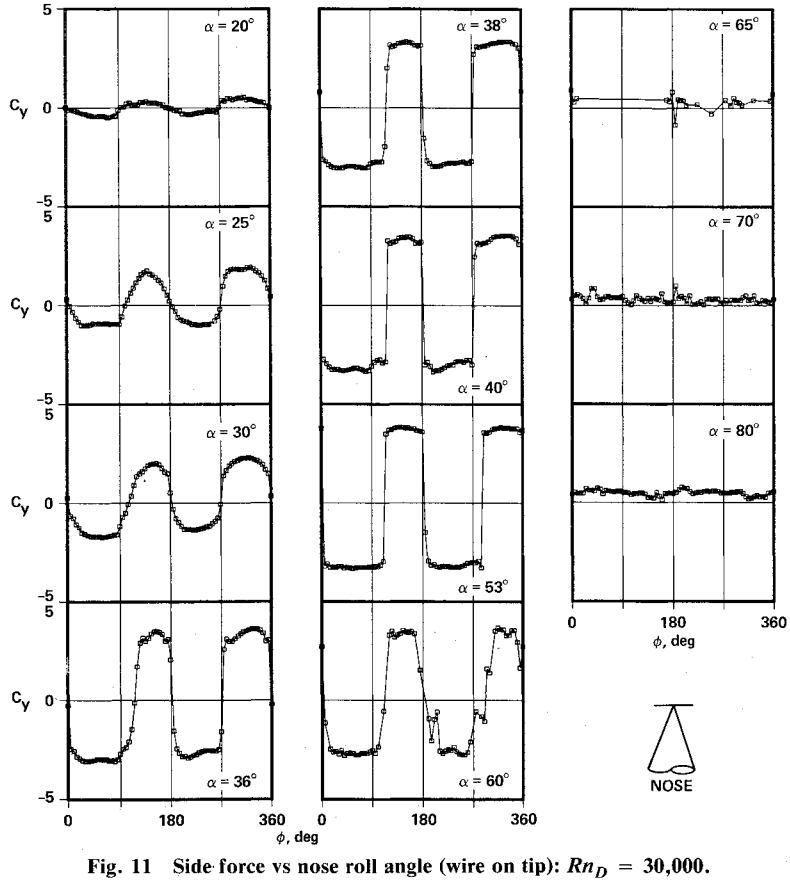

Fig. 11 Side force vs nose roll angle (wire on tip): Rn_D = 30,000.

forward part of the body and the other associated with the parallel shedding of vortices on the aft part. As α approaches 90 deg, regime 3, the steady asymmetric component, becomes essentially a pair of free vortices emanating from the tip, and regime 1, the parallel shedding of vortices, becomes essentially the entire unsteady component.

Tip Geometry Effects

The observed leeside flowfield behavior on a body of revolution at incidence has often been explained in terms of the impulsive flow analogy. The basic form of the analogy relates the axial steady, three-dimensional, growth of the flowfield around a pointed body of revolution to the time-dependent, two-dimensional flow past an impulsively started cylinder. It has generally been conceded that this analogy, which is an extension of the independence principle,[12] gives a qualitative description of the leeside flowfield development (see Ref. 13), but is not quantitatively accurate. The primary reason for the shortcomings of the analogy is that no upstream influence of the pressure field is permitted. An implication of the analogy

is that the flowfield on a pointed body of revolution is symmetric very close to the tip where the crossflow Reynolds number is less than approximately 50 and becomes asymmetric farther downstream.

Based on the results of the tip alterations and also smoke visualizations of the tip flow using a high-magnification lens, it is believed that the impulsive flow analogy description of the near-tip flowfield behavior is incorrect. A more probable description of the tip flowfield development is that, under the correct conditions ($\alpha > 30$ deg for $L/D = 16$ body), microasymmetries in the geometry of the tip act as an instability trigger. The size of the microasymmetries necessary to trigger the instability is dependent on the local body diameter. In addition, once the instability has been set off, the asymmetry propagates upstream to the tip through the pressure field and also, of course, downstream.

The actual orientation that the leeside vortices initially assume is highly dependent on the size and location of the microasymmetries at low angles of attack and dependent to a lesser degree at higher incidence angles. At higher angles (50 deg $< \alpha <$ 65 deg), the flowfield is bistable or nearly bistable, and its left-hand or right-hand orientation is established by the dominant features of the tip geometry. Evidence of this behavior can be found by comparing Fig. 3 with Figs. 11 and 12. At equivalent angles of attack, the levels of flowfield asymmetry at the higher angles of attack ($\alpha = 35$ deg) are more or less the same even though the tip geometry has been significantly altered, whereas at the lower angles, the continuous nature of the side-force measurements indicate that the vortices of the leeside flowfield have many orientations and respond to all of the tip microasymmetries present.

In the absence of tip perturbations the question arises whether other perturbations farther downstream may also act to trigger the asymmetric flowfield. This is possible, provided that the downstream perturbation be sufficiently large. One can imagine that a minute perturbation at the tip will activate growth of the asymmetry in the flowfield immediately behind it, which in turn will activate that of the succeeding flowfield, and so forth downstream. In the absence of a tip perturbation any one of these activated flowfields could be considered an appropriate trigger for succeeding flowfields. However, it is clear that, to achieve the same effect as the tip perturbation, the trigger would have to be very large. This condition may have been the source of the seeming contradiction between the finding of Dexter and Hunt[7,8] and that of Keener[9] concerning the effect on side force of altering the roll-angle position of the cylindrical afterbody. The negative finding of Dexter and Hunt compared to that of Keener may have been simply the result of too small a perturbation.

It was found to be possible to regularize the asymmetric flowfield by imposing planes of symmetry at the tip. The imposition of symmetry planes makes predictable the nose roll angles at which zero crossings of the side force are to be expected. Attaching a small cylinder to the tip has the potential of yielding zero crossings of the side force with every 90-deg change in nose roll angle. Attachment of a cylinder is appealing from the standpoint of analysis, inasmuch as the perturbed flowfield that it creates can be characterized by the same three regimes that were found useful in characterizing flow past the body itself. Machining flats at the tip yielded a similar result for the zero crossings of the side force, but had a curious effect, as yet unexplained, on the magnitude of the side force between zero crossings. Machining flats at the tip made it act, in effect, as a lifting flat-top body. It is possible that, when the sharp edges introduced by the flats were in proximity to the naturally occurring separation lines, they interfered with the initial development of the asymmetric flowfield.

Bistable States and "Regular" Configurations

Experimental results confirm the existence of bistable or nearly bistable states both for bodies having "natural" tips and tips with imposed symmetry planes. This result confirms that, under certain conditions, the orientation of the vortex-dominated leeside flowfield is a question of stability.

We note that, for a finite-length body, the flow at low to moderate values of α is dominated by the vortices emanating from the tip, whereas the shed vortices dominate as α approaches 90 deg. The side-force variation with roll-angle position of the nose changes accordingly from continuous at low

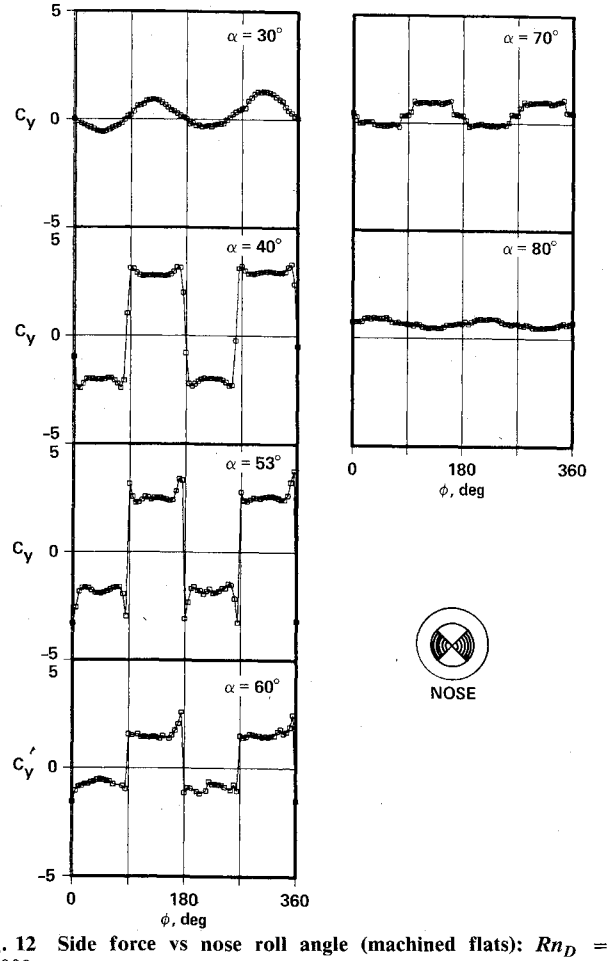

Fig. 12 Side force vs nose roll angle (machined flats): Rn_D = 30,000.

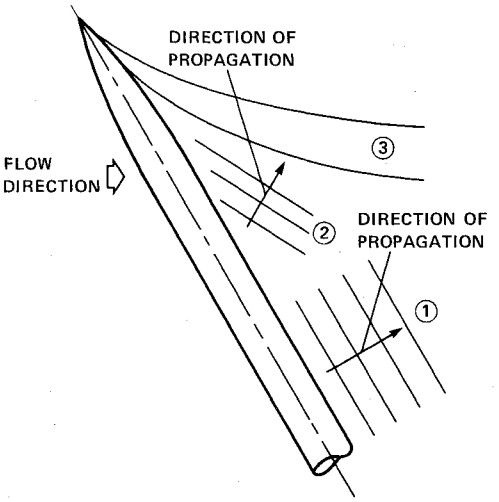

Fig. 13 Schematic of the leeward-side flow regimes.

to moderate α to a square-wave pattern for larger α. Finally, we note again that, as α approaches 90 deg, regime 3, the regime consisting of an asymmetric steady flow, becomes confined to an ever-diminishing zone just behind the nose. The magnitude of the square-wave pattern of side-force characteristic of this regime therefore approaches zero as α approaches 90 deg.

With gross alterations of the tip geometry, it is possible to obtain some steady intermediate flowfield configurations under conditions in which no such intermediate configurations exist for the natural or slightly altered tip. The discrepancy on this point between the results for the natural nose of the present study and results of other studies[5-8] is probably due to experimental technique. The technique used in Refs. 5–8 to determine the side force involved the integration of surface pressure measurements that were acquired over a period of time. In the present study, at certain critical nose-roll angles, time histories of the side force indicated that the flowfield did not have a stable mean. Visualizations of the flowfield showed that the leeward-side vortices were switching from side to side in a seemingly unpredictable manner. Under such conditions, averaging of the flowfield response over an interval of time can lead to an erroneous measurement that could be misinterpreted as evidence of an intermediate steady flowfield configuration.

The existence of a bistable flowfield is tantamount to the existence of regular states, as reported by Dexter and Hunt.[7,8] At incidence angles in the range of 40–60 deg, nearly constant values of side force are sustained over large nose roll-angle changes. A comparison of Figs. 3, 12, and 13 shows that, at $\alpha = 53$ deg, the magnitudes of the extremes in side force for the three nose geometries are nearly equal. Additionally, these were the largest magnitudes measured during the incidence angle sweeps. This supports the second aspect of a regular state as defined by Dexter and Hunt[7,8]: The extremes of side-force magnitude are essentially independent of tip geometry. The existence of extremes of side-force magnitude that are independent of tip geometry and of a maximum of all extremes both are consistent with the hypothesis that the tip vortices become virtually independent of the flow beneath them. Since the magnitude of their contribution to the side force becomes dominant as α increases from small values, but must approach zero as α approaches 90 deg, it is natural that a maximum of all magnitudes should exist at some particular value of α.

Conclusions

The results discussed herein help focus the picture of the asymmetric vortex flowfield on the leeward side of a pointed body of revolution at incidence. The principal conclusions can be summarized as follows:

1) The orientation of the leeward-side flowfield is strongly dependent on the tip geometry. Imposing symmetry planes at the tip makes predictable the nose roll angles at which zero crossings of the side force are to be expected. [Results of a recent study support this conclusion (see Ref. 14).]

2) The existence of a bistable, or nearly bistable, leeside flowfield indicates that the onset of asymmetric flow is a result of an instability mechanism.

3) At incidence angles ($\alpha > 65$ deg), the leeside flowfield consists of a steady vortex pair emanating from the tip, oblique shedding further down on the body, followed by shedding parallel to the axis of the body.

4) There are four angle-of-attack regimes that categorize the type of vortex behavior to be expected on pointed bodies of revolution. The regimes are symmetric leeward-side flow ($\alpha < 30$ deg), intermediate range ($30 < \alpha < 50$ deg) of steady asymmetric flow, nearly bistable range ($50 < \alpha < 65$ deg), and vortex shedding ($\alpha > 65$ deg).

References

[1]Degani, D., and Zilliac, G. G., "Experimental Study of Nonsteady Asymmetric Flow Around an Ogive-Cylinder at Incidence," *AIAA Journal*, Vol. 28, No. 4, 1990, pp. 642–649.

[2]Schiff, L. B., and Degani, D., "Numerical Simulation of Vortex Unsteadiness on Slender Bodies of Revolution at Large Incidence," AIAA Paper 89-0195, Jan. 1989.

[3]Degani, D., and Schiff, L. B., "Numerical Simulation of the Effect of Spatial Disturbances on Vortex Asymmetry," AIAA Paper 89-0340, Jan. 1989.

[4]Degani, D., "Numerical Investigation of the Origin of Vortex Asymmetry," AIAA Paper 90-0593, Jan. 1990.

[5]Lamont, P. J., "Pressures Around an Inclined Ogive Cylinder with Laminar, Transitional, or Turbulent Separation," *AIAA Journal*, Vol. 20, No. 11, 1982, pp. 1492–1499.

[6]Lamont, P. J., "The Complex Asymmetric Flow Over a 3.5 *D* Ogive Nose and Cylindrical Afterbody at High Angle of Attack," AIAA Paper 82-0053, Jan. 1982.

[7]Dexter, P. C., and Hunt, B. L., "The Effects of Roll Angle on the Flow over a Slender Body of Revolution at High Angle of Attack," AIAA Paper 81-0358, Jan. 1981.

[8]Hunt, B. L., and Dexter, P. C., "Pressures on a Slender Body at High Angle of Attack in a Very Low Turbulence Level Airstream," AGARD CP-247, Paper 17, 1978.

[9]Keener, E. R., Chapman, G. T., Cohen, L., and Taleghani, J., "Side Forces on a Tangent Forebody with Fineness Ratio 3.5 at High Angle of Attack and Mach Numbers 0.1 to 0.7," NASA TM-X-3437, 1977.

[10]Moskovitz, C. A., Hall, R. M., and DeJarnette, F. R., "Effects of Nose Bluntness, Roughness and Surface Perturbations on the Asymmetric Flow Past Slender Bodies at Large Angles of Attack," AIAA Paper 89-2236, Aug. 1989.

[11]Ramberg, S. E., "The Effects of Yaw and Finite Length upon the Vortex Wakes of Stationary and Vibrating Cylinders," *Journal of Fluid Mechanics*, Vol. 128, 1983, pp. 81–107.

[12]Jones, R. T., "Effects of Sweepback on Boundary-Layer and Separation," NACA Rept. 884, 1947.

[13]Zilliac, G. G., "Computational/Experimental Study of the Flowfield on a Body of Revolution at Incidence," *AIAA Journal*, Vol. 27, No. 8, 1989, pp. 1008–1016.

[14]Moskovitz, C., Hall, R., and DeJarnette, F., "Experimental Investigation of a New Device to Control the Asymmetric Flowfield on Forebodies at Large Angles of Attack," AIAA Paper 90-0069, Jan. 1990.